

## Electronic Supplementary Information

### Synergetic Effect of MoS<sub>2</sub> and Graphene on Ag<sub>3</sub>PO<sub>4</sub> for its Ultra-Enhanced Photocatalytic Activity in Phenols Degradation under Visible Light

Wen-chao Peng <sup>1</sup>, Xi Wang <sup>1,2</sup> and Xiao-yan Li <sup>1\*</sup>

<sup>1</sup> Environmental Engineering Research Centre, Department of Civil Engineering,  
The University of Hong Kong, Pokfulam Road, Hong Kong

<sup>2</sup> School of Chemistry and Environment, South China Normal University, Guangzhou,  
Guangdong, China

(\*Corresponding author: phone: 852 2859-2659; fax: 852 2859-5337; e-mail: [xlia@hkucc.hku.hk](mailto:xlia@hkucc.hku.hk))

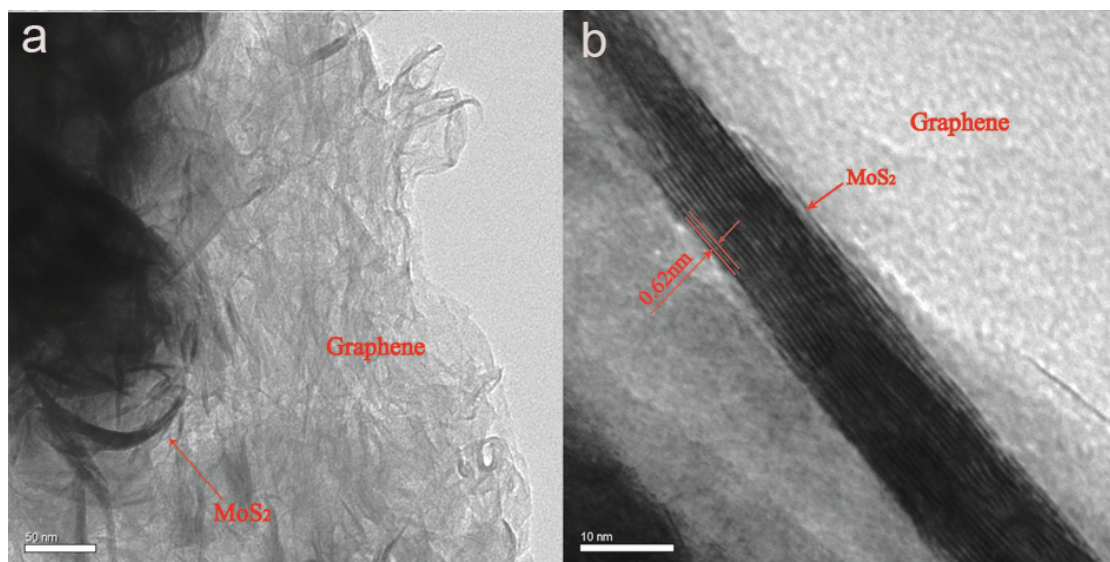


Fig. S1. Morphology of the MoS<sub>2</sub>/GR hybrid: (a) TEM images in large magnifications of the layered MoS<sub>2</sub>/GR hybrid; (b) high-resolution TEM image of the hybrid showing the close contact between the MoS<sub>2</sub> and GR.

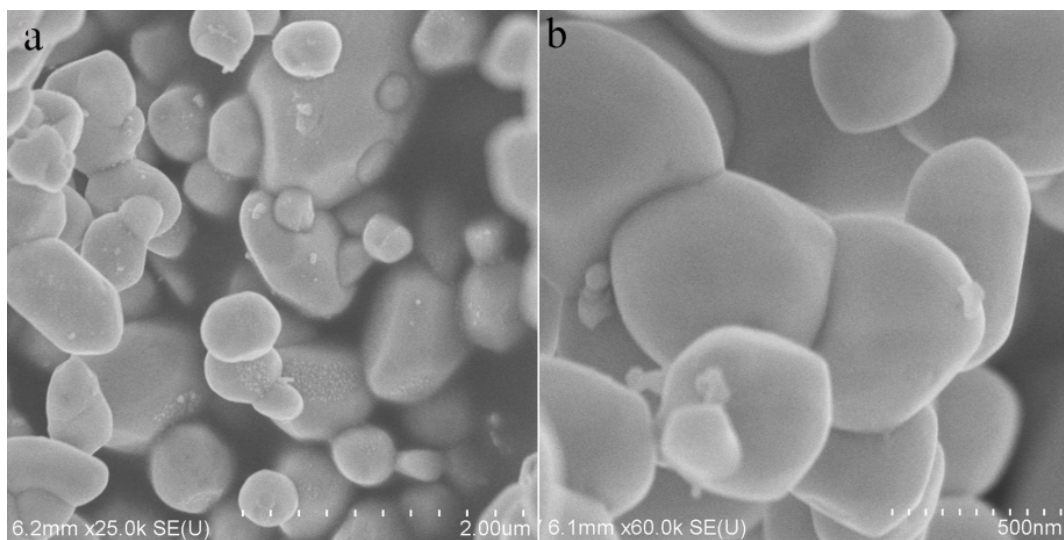


Fig. S2. (a) and (b) SEM images of the pure  $\text{Ag}_3\text{PO}_4$  crystals at different magnifications

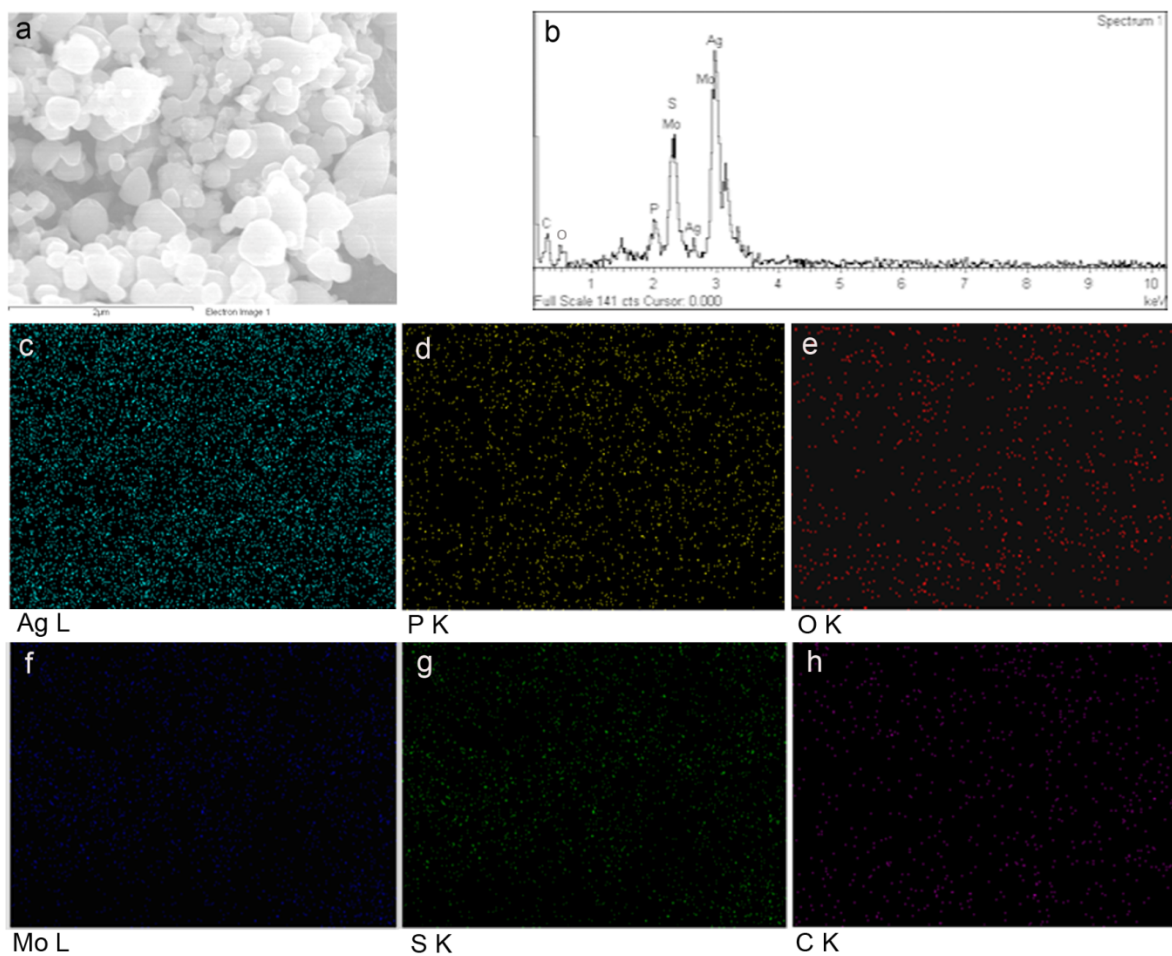


Fig. S3. Elemental analysis for  $\text{Ag}_3\text{PO}_4\text{-MoS}_2/\text{GR}$  composite: (a) SEM image of the mapping area; (b) EDX spectra of the  $\text{Ag}_3\text{PO}_4\text{-MoS}_2/\text{GR}$  composite; (c)-(h) EDX elementary mapping of Ag, P, O, Mo, S and C in  $\text{Ag}_3\text{PO}_4\text{-MoS}_2/\text{GR}$  composite.

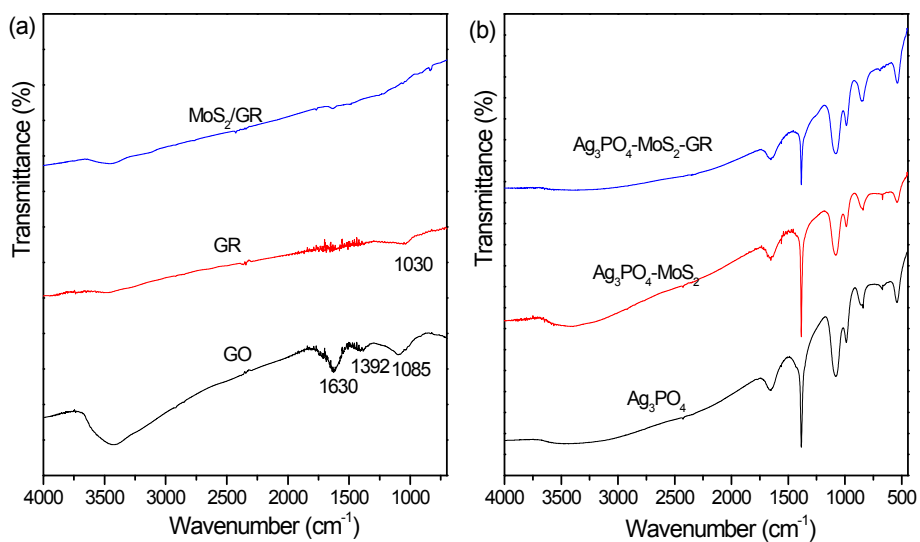


Fig. S4. (a) FT-IR spectra of the GO, GR and MoS<sub>2</sub>/GR hybrid (note: most of the functional groups were removed for the GO, indicating a successful reduction from GO to GR); (b) FT-IR spectra for the pure Ag<sub>3</sub>PO<sub>4</sub> and composites (note: there were no new chemical bonds formed during the composite preparation process).

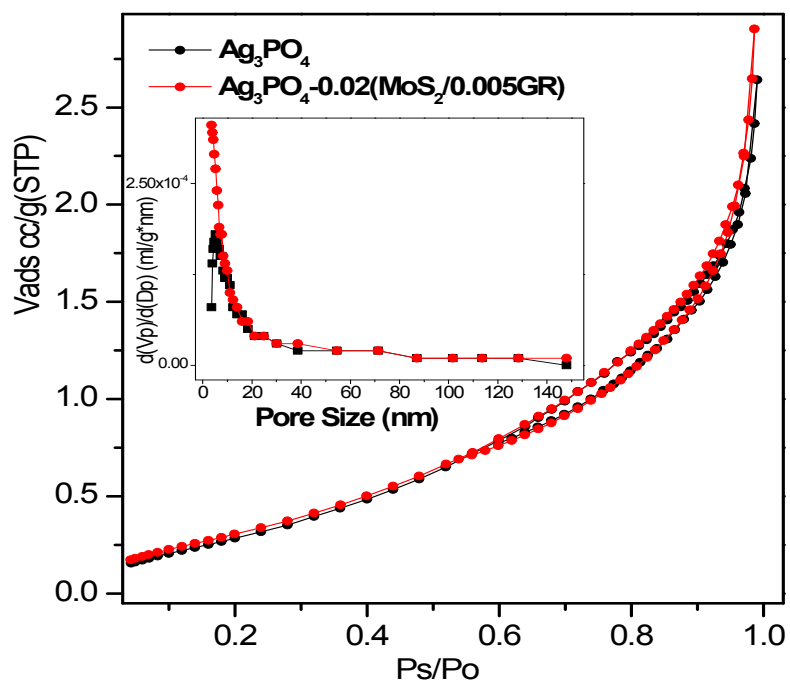


Fig. S5. N<sub>2</sub> adsorption tests for the pure Ag<sub>3</sub>PO<sub>4</sub> and Ag<sub>3</sub>PO<sub>4</sub>-MoS<sub>2</sub>/GR composite. A slight increase in adsorption capability was found after the MoS<sub>2</sub>/GR addition. However, the pore structure was nearly the same. The surface areas of Ag<sub>3</sub>PO<sub>4</sub> and Ag<sub>3</sub>PO<sub>4</sub>-0.02(MoS<sub>2</sub>/0.005GR) composite were 1.1 and 1.2 m<sup>2</sup>/g, respectively, and the total pore volumes (Ps/Po = 0.9814, Adsorption) were 0.0035 and 0.0040 ml/g for these two respective photocatalyst materials.

## Photoelectric Conversions

The photoelectric conversion property was investigated on the photocatalyst materials using a three-electrode cell connected to a computer-controlled potentiostat (Princeton VersaSTAT 4). To make a working electrode for a catalyst material, 50 mg of the catalyst powder, 2.5 mg carbon black and 5 mg polyvinylidene difluoride (PVDF) were first mixed into 0.5 mL N,N-Dimethylmethanamide (DMF). The mixture was ultrasonically dispersed for 15 min, and 0.1 mL of the solution was then dropped on a tin-doped indium oxide (ITO) glass slide (1.5×1 cm). After evaporation of the DMF, the catalyst was left that attached firmly onto the surface of the ITO glass. For the photocurrent measurement on the working electrode, a Pt film (2×1 cm) was used as the counter-electrode, an Ag/AgCl electrode was used as the counter-electrode, and all three electrodes were immersed in 0.01 M sodium sulfate as the electrolyte. The light source had a 300W Xe lamp with a cutoff filter of 420 nm inserted for the visible-light irradiation. The photocurrent density was detected by the potentiostat, and the current-time (i-t) curves were obtained without bias.

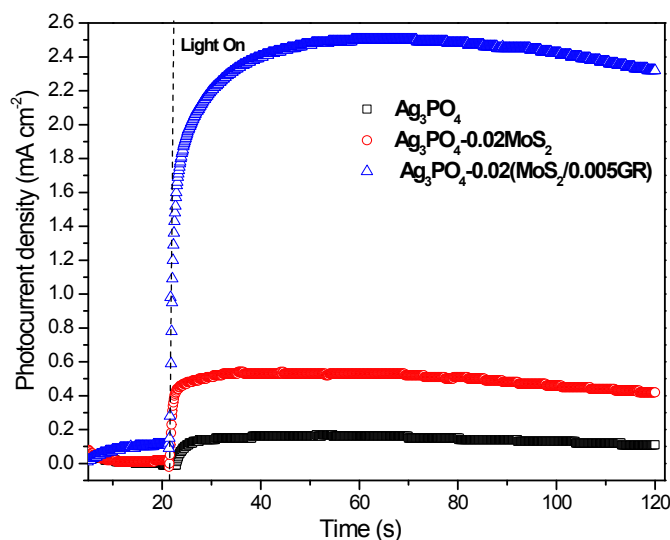


Fig. S6. The transient photocurrents of the Ag<sub>3</sub>PO<sub>4</sub>, Ag<sub>3</sub>PO<sub>4</sub>-MoS<sub>2</sub> and Ag<sub>3</sub>PO<sub>4</sub>-MoS<sub>2</sub>/GR electrodes in 0.01 M Na<sub>2</sub>SO<sub>4</sub> aqueous solution under visible light ( $\lambda > 420$  nm) without bias versus Ag/AgCl as the reference electrode.

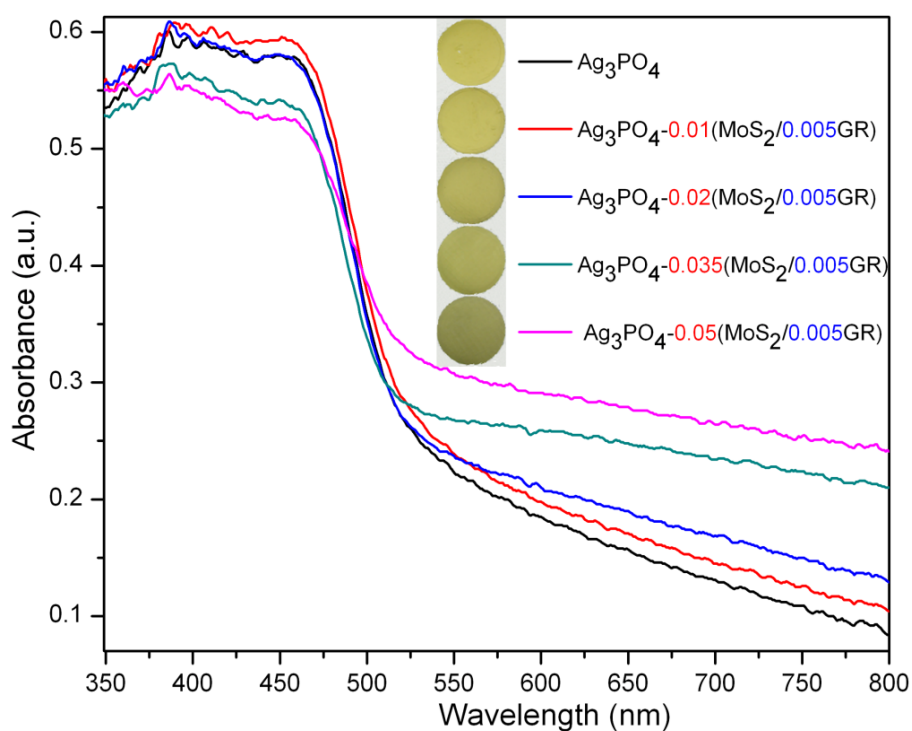


Fig. S7. UV-vis diffusive reflectance spectra of the Ag<sub>3</sub>PO<sub>4</sub> and Ag<sub>3</sub>PO<sub>4</sub>-MoS<sub>2</sub>/GR composites. The composites exhibited a stronger absorption capability in the visible light region as the MoS<sub>2</sub>/GR co-catalyst content increased. This was in agreement with the color change of the composites from light green to dark green, as indicated by the inset images.

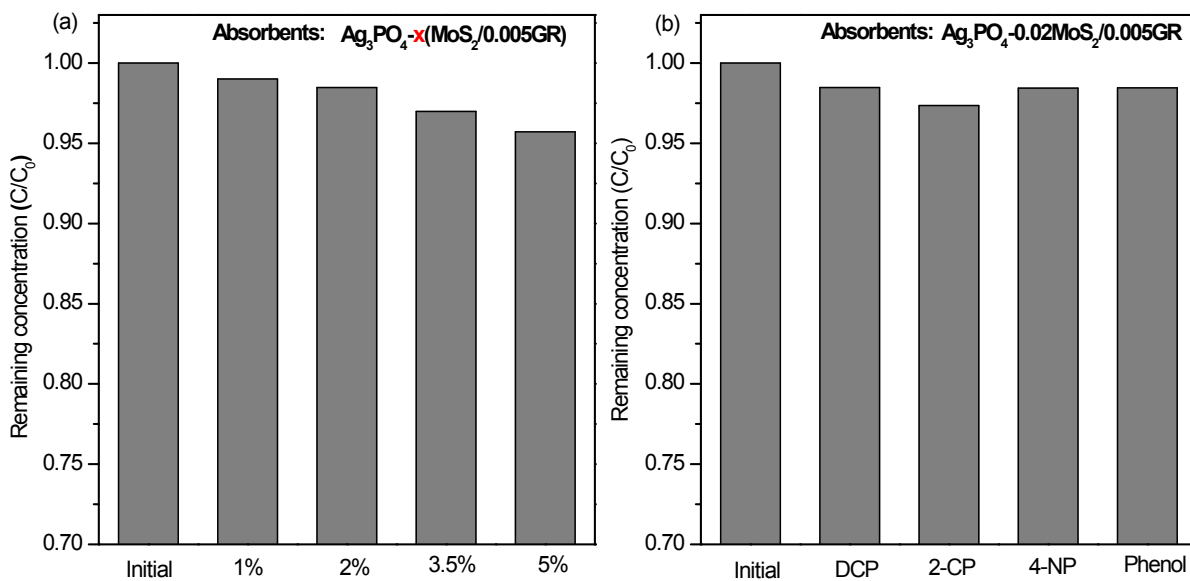


Fig. S8. (a) Change in DCP concentration after adsorption in the dark by the  $\text{Ag}_3\text{PO}_4$ -based catalysts with different  $\text{MoS}_2/0.005\text{GR}$  percentages; (b) Change in concentration for different phenols after adsorption in the dark by  $\text{Ag}_3\text{PO}_4\text{-0.02}(\text{MoS}_2/0.005\text{GR})$ .

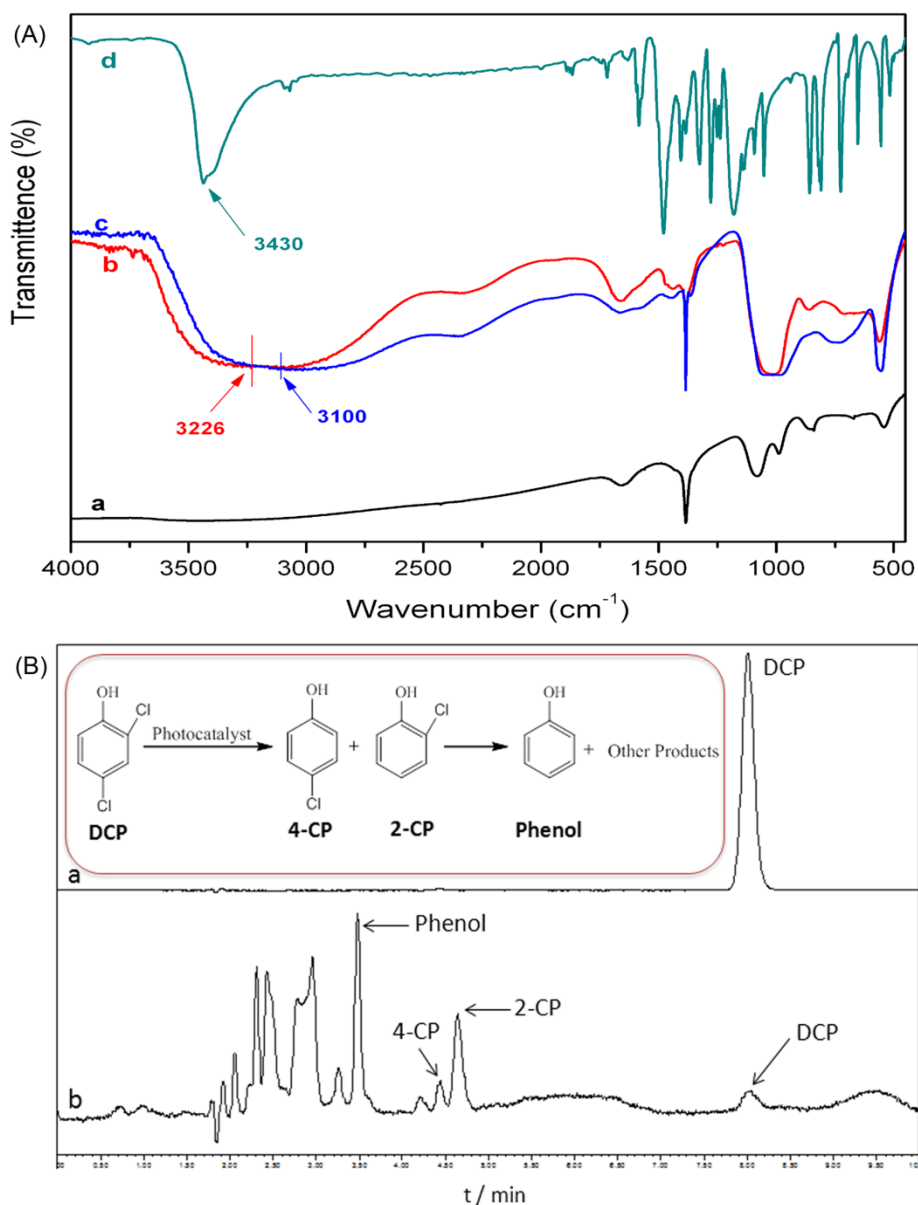


Fig. S9 (A) FT-IR spectra of (a) the Ag<sub>3</sub>PO<sub>4</sub>-0.02(MoS<sub>2</sub>/0.005GR) photocatalyst suspension, (b) Ag<sub>3</sub>PO<sub>4</sub>-0.02(MoS<sub>2</sub>/0.005GR) photocatalyst mixing in the DCP solution in the dark for 4 h, (c) Ag<sub>3</sub>PO<sub>4</sub>-0.02(MoS<sub>2</sub>/0.005GR) photocatalyst mixing in the DCP solution in the dark for 4 h and then under visible light for 1 h, and (d) pure DCP solution; (B) HPLC spectra of the DCP solution (a) before degradation and (b) after the photo-degradation; inset of Fig. B is the proposed mechanism of photocatalytic DCP degradation.

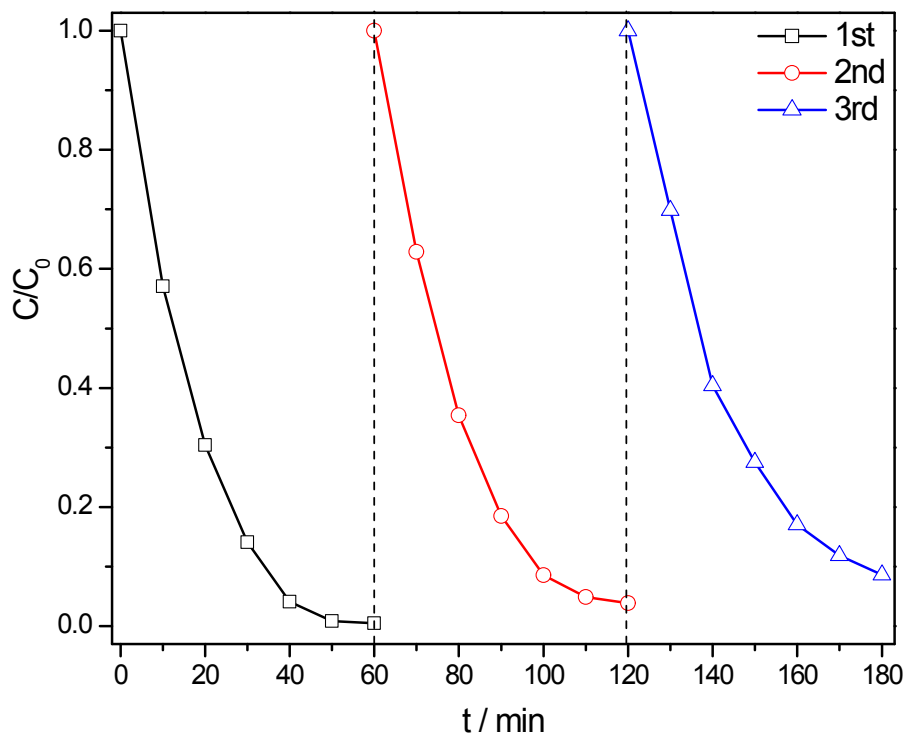


Fig. S10. The stability and reactivity of the recycled  $\text{Ag}_3\text{PO}_4\text{-}0.02(\text{MoS}_2/0.005\text{GR})$  catalyst as demonstrated by the repeated tests of photocatalytic DCP degradation.

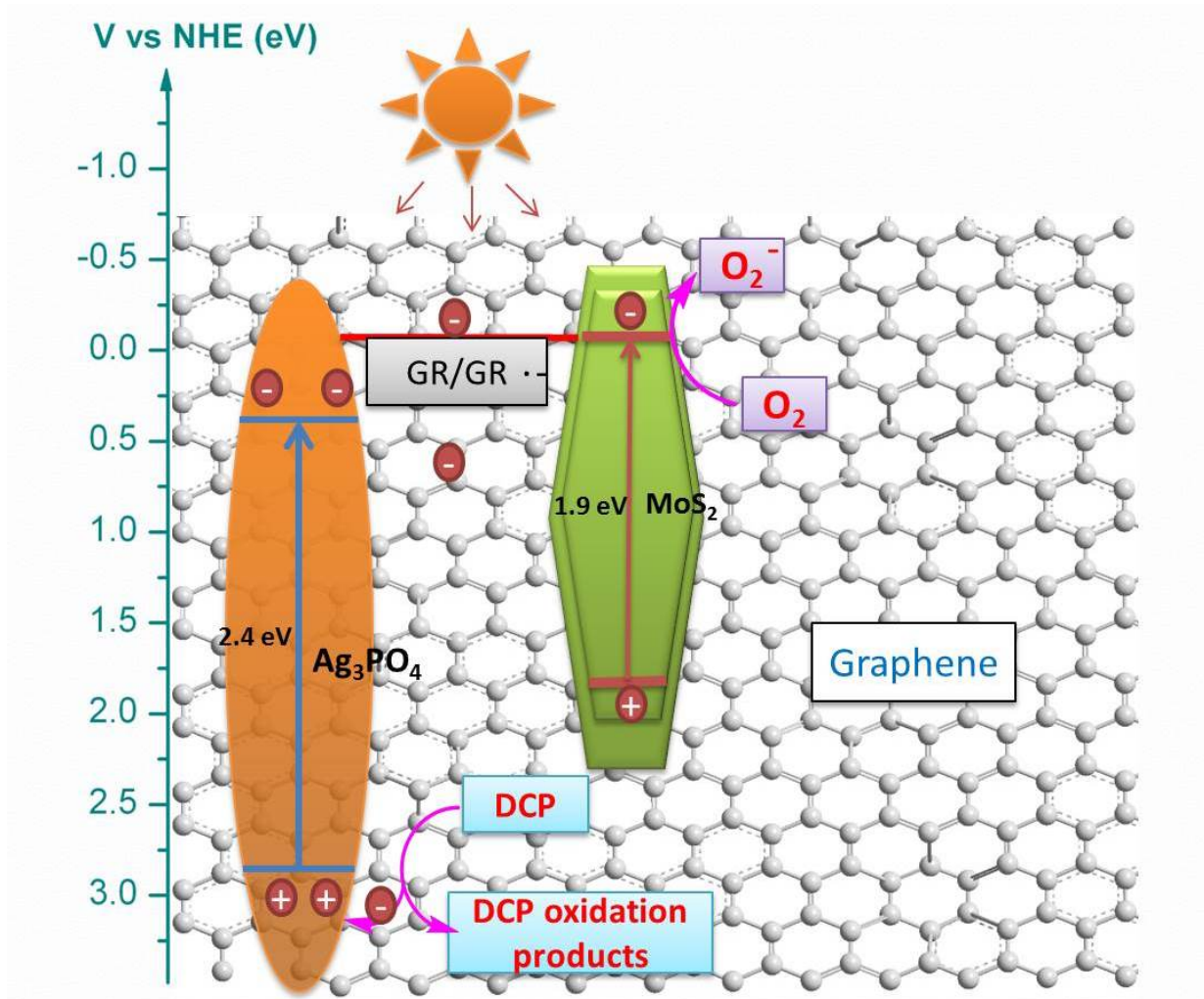


Fig. S11. Schematic illustration of the energy diagram and electron transfer scheme for the photocatalytic DCP degradation by the  $\text{Ag}_3\text{PO}_4\text{-MoS}_2/\text{GR}$  composite.